Measurement of Omnidirectional Light Distribution by a Mirrored Ball

Shoji Tominaga and Norihiro Tanaka
Osaka Electro-Communication University, Department of Engineering Informatics
Neyagawa, Osaka, Japan

Abstract

Illuminant estimation in natural scenes includes the problem of estimating a spatial distribution of light sources by omnidirectional observations. The present paper describes a method for estimating an omnidirectional light distribution from the image of a camera aiming at a mirrored ball. The parameters including the camera location in the scene and the focal length of the camera lens are estimated to precisely determine the mapping between coordinates on the ball and light rays in the world. We create two types of image to represent the omnidirectional light distribution in the world. One representation is a polar coordinate system with the origin located at the center of the mirrored ball. The other is a parallel projection on a two-dimensional screen passing the center of the ball. Experiments in a natural scene using a spherical steel ball and a color CCD camera are described. First, we estimate an omnidirectional radiance distribution indoors in a room with fluorescent ceiling lights. Second, we estimate the radiance distribution in the open air. The scene includes strong specular high light by direct reflection of sunlight. We analyze the chromaticity of the omnidirectional light source.

Introduction

Knowing the scene illumination is very important for visual experiments related to color appearance, color constancy, and color adaptation, and also in color engineering such as color reproduction, color correction, and color measurement. Recently in the fields of computer graphics and computer vision a variety of methods were proposed for estimating scene illumination for realistic image rendering and image understanding. Most of the estimation methods assumed a single illumination source.

Many illumination sources are present in natural scenes. The case of one source seldom happens. For example, an indoor scene may have electric light sources of ceiling lamps, table lamps, and natural light source through windows. An outdoor scene may have the direct illumination source of sunlight and the second source of blue sky. Hubel[1] made an interesting observation about the perception of object color lit by sunlight at dawn and dusk. When the light of the setting sun illuminates an object or person, the surfaces impart a characteristic warm glow. An indoor scene illuminated by tungsten light of identical color temperature and spectral distribution to the sunset light does not give any similar perception. The visual system can distinguish a scene lit by the sunset light from the scene by the tungsten light. He explained that the color gamut observed in these conditions is larger than the gamut under a single illumination source. The main objects in the scene are illuminated by the direct sunlight and the shadows are illuminated by a second source of the blue sky.

Therefore, illuminant estimation in natural scenes includes the problem of estimating a spatial distribution of light sources by omnidirectional observations. Previous omnidirectional measuring systems used a mirrored ball,[2] a fisheye lens,[3] and a mirror with a hyperbolic curve.[4] Debevec[2] developed a technique for using a mirrored ball in CG, called a light probe, to acquire an omnidirectional image that records the illumination conditions at a particular point in space. Such images were used for compositing objects into actual photography of a scene. However his paper did not explain the camera calibration that is needed to precisely determine the illumination distribution. The fisheye lens is mounted directly on a camera, but the viewing range is narrower than the ball. Since the mirror with a hyperbolic curve was developed for robot vision, viewing the sky was neglected.

The present paper describes a method for estimating an omnidirectional light distribution from the image of a camera aiming at a mirrored ball. We calibrate the imaging system. The parameters including the camera location in the scene and the focal length of the camera lens are estimated to precisely determine the mapping between coordinates on the ball and light rays in the world. We create two types of image to represent the omnidirectional light distribution in the world. One representation is a polar coordinate system with the origin located at the center of the mirrored ball. The other is a parallel projection on a two-dimensional (2D) screen passing the center of the ball. Experiments in a natural scene using a spherical steel ball and a color CCD camera are described.

Measuring System

Figure 1 depicts the geometric model for the measuring system using a mirrored ball. A camera aims at a spherical mirror, such as a polished stainless steel ball, placed at any

location in a natural environment. The camera photographs the spherical mirror to obtain an omnidirectional radiance map around the location. In the figure **N** is the surface normal, **L** is the light directional vector, and **V** is the viewing vector. Moreover, $\mathbf{V}_r$ is **V** mirrored about **N**. We assume that the ray beams from a light source are parallel. So the mirrored vector $\mathbf{V}_r$ is the same directional vector as the light vector **L** from the spherical center.

One of the advantages of this measuring system is that the observable range is much wider than the range of other omnidirectional systems, and the surrounding scenery of the ball for almost all directions can be acquired from a single image. Figure 2 shows the real observable range by the present system. The optical axis of the camera passes through the center of the ball, and let ψ be the visual angle of the hemisphere. Then the observable range is $360° - 2\psi$.

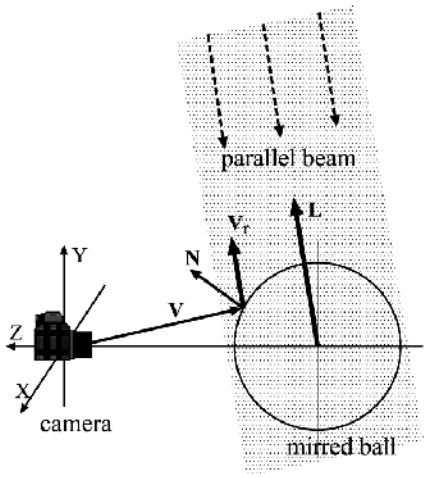

Figure 1 Measuring system using a mirrored ball.

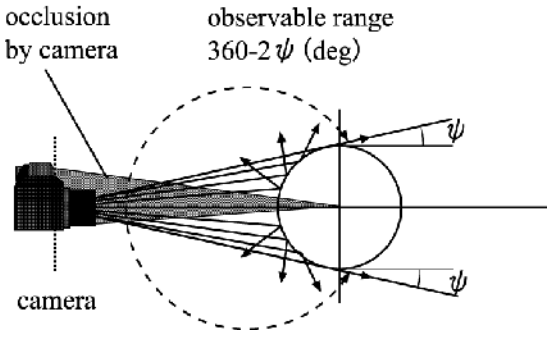

Figure 2 Observable range.

Camera Calibration

In order to determine precisely the mapping between coordinates on the spherical ball and rays in the world, we need to know the camera parameters including optical position in the scene and focal length. The camera is assumed to be a pinhole camera the image plane of which is composed of a set of square cells of CCD. Figure 3 shows projecting an object in a 3D space onto a screen by the camera in perspective. We call the system of coordinates (X, Y, Z) in the 3D space the world coordinate system, and call the system of coordinates (x, y) in the plane the screen coordinate system. The projection equation from the world coordinates to the screen coordinates is described as $\mathbf{P}\begin{bmatrix} X & Y & Z & 1 \end{bmatrix}^t = s\begin{bmatrix} x & y & 1 \end{bmatrix}^t$, where t stands for matrix transposition. The projection matrix **P** is defined as

$$\mathbf{P} = \begin{bmatrix} \alpha & 0 & x_0 & 0 \\ 0 & \alpha & y_0 & 0 \\ 0 & 0 & 1 & 0 \end{bmatrix}. \tag{1}$$

The coordinates (x_0, y_0) represent the optical axis that is the principal point on the image. Let f be the focal length and k be the pixel length. Then the generalized focal length is defined as $\alpha = f\,k$. The coefficient s is a normalization parameter. The parameters of the focal length α and the principal point (x_0, y_0) are intrinsic camera parameters.

We estimate the parameters according to the following procedure. Figure 4 shows an experimental setup for determining the camera parameters. Target objects A and B are of the same length L. These two reference objects project their images with different lengths on the screen in perspective. First, let l_A and l_B be the lengths of the respective obejcts projected on the screen. Then the projection for these objects must satisfy the following equations

$$\begin{aligned} \mathbf{P}\begin{bmatrix} 0 & L & D & 1 \end{bmatrix}^t &= s\begin{bmatrix} 0 & l_A & 1 \end{bmatrix}^t \\ \mathbf{P}\begin{bmatrix} 0 & L & D+d & 1 \end{bmatrix}^t &= s\begin{bmatrix} 0 & l_B & 1 \end{bmatrix}^t \end{aligned}, \tag{2}$$

where $(x_0, y_0)=(0, 0)$ is assumed. From these equation α is found as $\alpha = l_A l_B d \big/ L(l_A - l_B)$.

Next, the principal point (x_0, y_0) is estimated using the vanishing point. The vanishing point means the point, which is the image of the common point at infinity of the 3D lines.

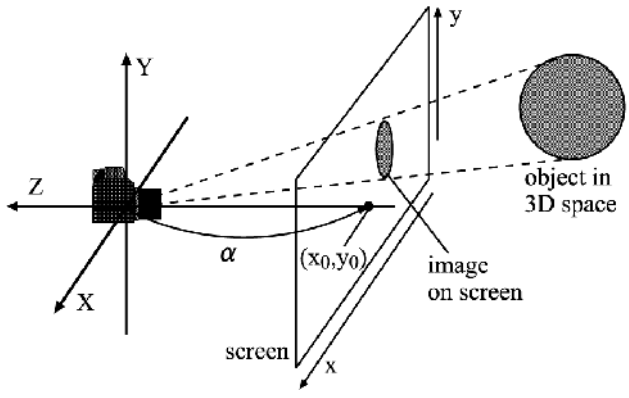

Figure 3 Perspective projection of an object.

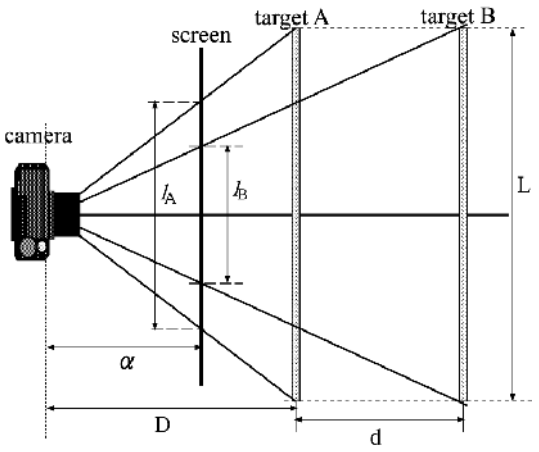

Figure 4 Setup for camera parameters.

Mapping from the Spherical Ball to the World

The radiance measurements observed from the spherical ball are mapped into light rays in the world. To perform this mapping we have to calculate the light vector **L** at any location on the ball. As the first step, the viewing vector **V** for the coordinates (x, y) on the image can be expressed using the camera parameters α and (x_0, y_0) as $\mathbf{V} = [x - x_0,\ y - y_0,\ -\alpha]^t$. Next, the light vector is estimated at every pixel of the ball image. This vector can be expressed in the form $\mathbf{L} = \mathbf{V}_r = \mathbf{V} - 2(\mathbf{N}^t \cdot \mathbf{V})\mathbf{N}$. Finally, the surface normal vector **N** is determined using the spherical property. Let r be the ball radius and (x_C, y_C) be the center coordinates on the image. The vector at (x, y) can be calculated by

$$\mathbf{N} = \left[x - x_c,\ y - y_c,\ \sqrt{r^2 - (x - x_c)^2 - (y - y_c)^2}\right]^t .$$

In order to represent the radiance spatial distribution, we create the two types of images: (A) polar coordinate representation and (B) orthographic projection representation.

(A) A set of the light vectors **L** points in all directions from the spherical center as shown in Figure 5. Therefore, assuming a camera at the spherical center, we can produce an omnidirectional image observed at the center point. Let (x_s, y_s, z_s) be the rectangular coordinates on the spherical ball the axis z_s of which is coincident with the optical axis Z. The light vector is expressed in the polar coordinates (θ, ϕ) by transformation

$$\theta = \tan^{-1}\left(y_s \Big/ \sqrt{x_s^2 + z_s^2}\right),\ \phi = \tan^{-1}\left(x_s / z_s\right). \quad (3)$$

Calculation of the radiance values looking in all directions of (θ, ϕ) provides the omnidirectional image mapped on a sphere.

(B) Mapping by orthographic projection onto a screen provides an image that is convenient for image analysis, although the viewing range is limited. Figure 6 depicts transformation for this projection. Assume that the center of the camera lens is at (0, 0, 0) and the optical axis directs (θ_0, ϕ_0) in the polar system. The screen crosses this axis at right angles. Let (x, y) be the screen coordinates. Then orthographic projection of any point (θ, ϕ) of the sphere into the screen is described as

$$x = r\cos(\phi + \phi_0)\cos(\theta + \theta_0),$$
$$y = r\sin(\phi + \phi_0)\cos(\theta + \theta_0). \quad (4)$$

This operation provides an orthographic image for the viewing direction (θ_0, ϕ_0).

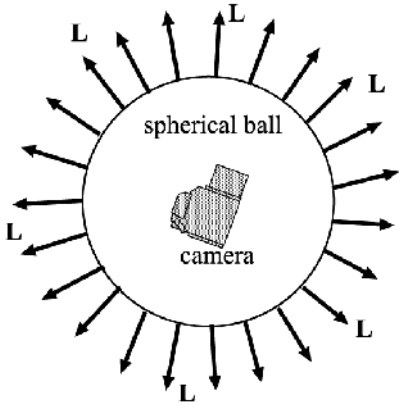

Figure 5 Light vectors around the ball.

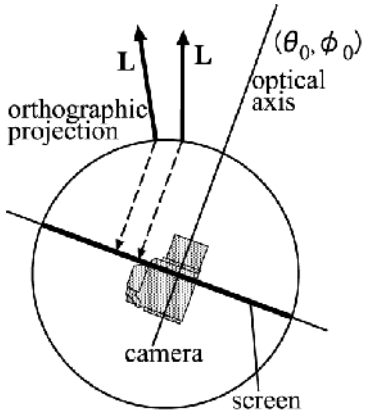

Figure 6 Orthographic projection representation.

To accurately estimate the light source from the observed image of the ball, one can correct the observed radiance based on the angle of incidence and the surface reflectance properties of the ball. The spectral radiance $Y(\lambda)$ of light reflected from a polished metal surface is described as

$$Y(\lambda) = \left(F(\theta_i, n(\lambda), k(\lambda)) \Big/ \cos(\theta_i)\right) E(\lambda), \quad (5)$$

where F represents the Fresnel spectral reflectance, θ_i is the angle of incidence, $k(\lambda)$ is the absorption coefficient,

$n(\lambda)$ is the index of refraction, and $E(\lambda)$ is the spectral distribution of the light source. For correction in estimating the light source, we apply the inverse function of Eq.(5) to the observed radiance. Using the optical data of an inhomogeneous dielectric material we can approximate the Fresnel reflectance of the stainless steel. In this study it is assumed that $n(\lambda)$ =1.7 and $k(\lambda)$ =0.0, and the spectral reflectance is constant over the range of visible wavelength. That is, the correction was done with respect to the incident angle only.

Experimental Results

First, we estimated an omnidirectional radiance distribution indoors in a room with fluorescent ceiling lights. Figure 7 shows the image of the stainless steel ball with radius of 6 cm. The visual angle for the hemisphere is $\psi = 5.7°$, and the observable range is $348.6°$. Figure 8 shows the omnidirectional image in polar coordinates (θ, ϕ). In this mapping process, we sub-sampled the observed image using a spline interpolation to increase resolution ten times. Figure 9 shows the radiance directional distribution, where the radiance is depicted with the length of color vector $\left(R^2 + G^2 + B^2\right)^{1/2}$. We can see some directions of the main light source. The bright light source is classified into four groups. The validity of this result is confirmed from the arrangement of fluorescent lamps on the ceiling in Figure 7.

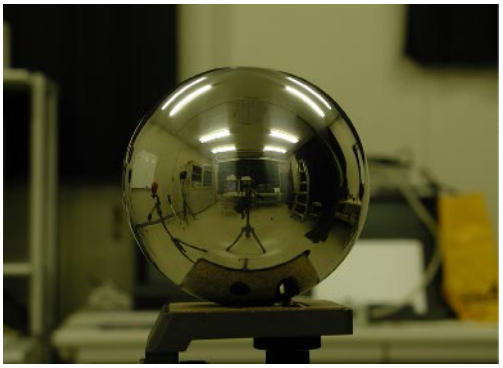

Figure 7 Steel ball is shown indoors.

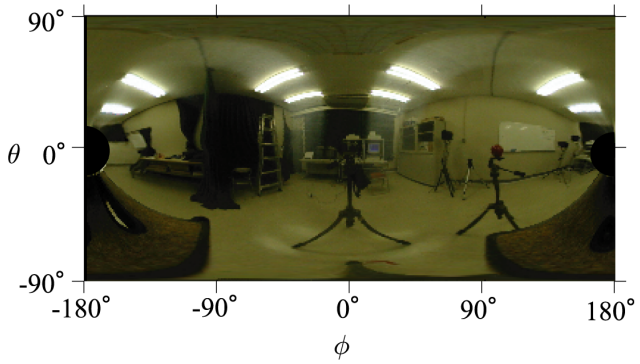

Figure 8 Omnidirectional image.

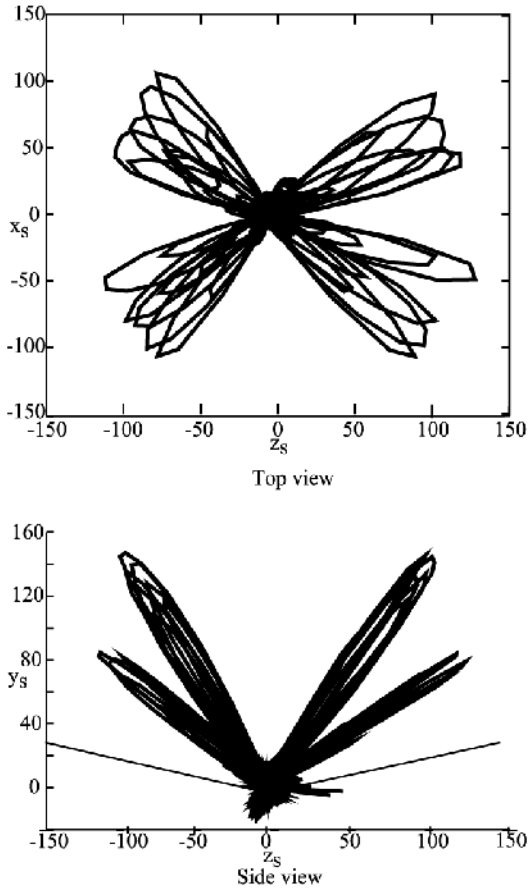

Figure 9 Radiance directional distribution.

Figure 10 Steel ball in an outdoors scene.

Second, we estimated an omnidirectional radiance distribution in the open air. Figure 10 shows the steel ball, which was placed on the roof of our building under a clear sky. The scene includes strong specular high light by direct reflection of sunlight. To acquire high dynamic-range images of this scene, three images of this scene were taken with the camera in three shutter speeds of 1/500th, 1/1000th, and 1/2000th of a second, and then a scaling was used to

combine the three images. Figure 11 shows a 3D perspective view of the radiance directional distribution, where the origin of (x_s, y_s, z_s) is the center of the ball.

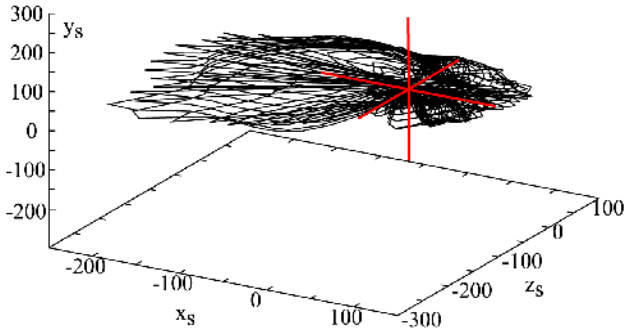

Figure 11 Radiance distribution outdoors.

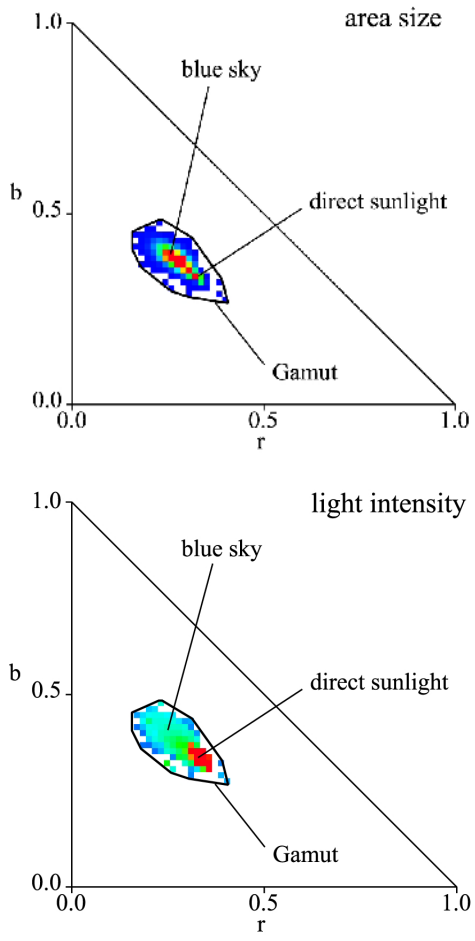

Figure 12 Gamut and distribution of light source on chromaticity diagram (r, b).

Figure 12 shows the chromaticity coordinates $(r, b) = (R/(R+G+B), B/(R+G+B))$ for the omnidirectional light source. In both graphs the whole light source is depicted as the convex hull of all chromaticity coordinates. The upper graph represents the chromaticity distribution based on area size with the same chromaticity. The gradation from red to blue means a decrease in the area size with the same chromaticity. The lower graph represents the chromaticity distribution based on light intensity. These graphs suggest the difference between direct sunlight and blue sky. The direct sunlight is very bright and somewhat reddish in the gamut. Most of the light comes from blue sky. Therefore we cannot neglect this source in color image analysis although it is much darker than the direct sunlight.

We are currently developing a measuring system and algorithms for estimating illuminant spectra of an omnidirectional light source.

Conclusion

This paper has described a method for estimating an omnidirectional light distribution from the image of a camera aiming at a mirrored ball. We calibrated the imaging system carefully. The parameters including the camera location in the scene and the focal length of the camera lens were estimated to determine the mapping between coordinates on the ball and light rays in the world. We created two types of image to represent the omnidirectional light distribution in the world. One representation was a polar coordinate system with the origin located at the center of the mirrored ball. The other was a parallel projection on a two-dimensional screen passing the center of the ball. Experimental results in a natural scene were presented using a spherical steel ball and a color CCD camera. First, an omnidirectional radiance distribution was estimated indoors in a room with fluorescent ceiling lights. Second, the radiance distribution was estimated in the open air, including strong direct sunlight. The gamut and distribution of light source could be analyzed on chromaticity diagram.

The authors thank Brian A. Wandell for his useful comments and discussions in this work.

References

1. P.M. Hubel: The perception of color at dawn and dust, Proc. The Seventh Color Imaging Conf.: Color Science, Systems, and Applications, pp.48-51,1999.
2. P. E. Debevec: Rendering Synthetic Objects into Real Scenes: Bridging Traditional and Image-based Graphics with Global Illumination and High Dynamic Range Photography, Proc. SIGGRAPH 98, pp.189-198, 1998.
3. I. Sato, Y. Sato, and K. Ikeuchi: Acquiring a radiance distribution to superimpose virtual objects onto a real scene, IEEE Tran. Visualization and Computer Graphics, Vol.5, No.1, pp.1-12, 1999.
4. K. Yamazawa, Y. Yagi, and M. Yachida: Omnidirectional imaging with hyperboloidal projection, Proc. Int. Conf. On Intelligent Robotics and Systems, pp.1029-1034, 1993.